




# Regulating the higher harmonic cutoffs via sinc pulse

Rambabu Rajpoot <sup>\*</sup>, Amol R. Holkundkar <sup>†</sup> and Jayendra N. Bandyopadhyay <sup>‡</sup>  
Department of Physics, Birla Institute of Technology and Science - Pilani, Rajasthan, 333031, India  
(Dated: June 27, 2022)

We theoretically investigate the generation of higher harmonics and the construction of a single attosecond pulse by means of two oppositely polarized sinc-shaped driver pulses. In comparison to a few-cycle Gaussian pulse of the same energy, here we observe a significant broadening in the bandwidth of an XUV/soft-Xray supercontinuum spectrum in the synthesized pulse. Furthermore, we observe that the harmonic cutoff and its corresponding intensity follow a well-defined scaling with the *delay parameter* between the two pulses. In principle, this delay can easily be tuned in on an optical bench. The typical nature of the synthesized pulse ensures the generation of single attosecond pulse instead of a pulse train. In this case, we obtain a single attosecond pulse of duration  $\sim 27$  as in XUV/soft-Xray regime of the electromagnetic spectrum. Depending on the delay parameter we observe an enhancement in some satellite harmonics. The proposed setup promises a highly tunable source of energetic photons, wherein the energy of the photons can easily be controlled from XUV to soft-Xray regime by simply changing the delay between two oppositely polarized sinc-pulses.

## I. INTRODUCTION

The last decade has witnessed rapid development in the field of higher harmonic generation (HHG), both in experimental and theoretical front [1]. The HHG and, consequently the production of attosecond pulses (ASPs) have enabled researchers to probe the fundamental processes of atomic and molecular phenomenon with unprecedented resolution. The ASP is particularly important for investigating the electron correlation effects and observing characteristic temporal delays in photoemission from different atomic orbitals [2, 3]. The ASP can also probe detailed microscopic motion of electrons in atoms, molecules, or any other nanoscale structures, and those effectively bridge the gap between various fields of basic sciences [4–8].

The HHG originates from the interaction of intense laser with gas atoms, which leads to the generation of coherent radiation at higher harmonics of the laser frequency. Experimentally, it has been observed that Higher Harmonic spectrum consists of a plateau where harmonic intensity is nearly constant over many orders of magnitude followed by a sharp cutoff [9, 10]. Ever since the inception of the idea of the generation of the higher harmonics by laser-atom interaction, the research objectives around the globe are aimed towards the enhancement of the harmonic cutoff of the HHG and also to increase the corresponding intensity of the emitted harmonics. There are various studies devoted to achieve these goals. The effect of the pulse chirp [11–16], pulse duration [17–19], synthesis of laser pulse using two or more colors laser fields [20–24], plasmonic fields [25–28] on the harmonic cutoff and the intensity of the emitted harmonics is reported in the past. Moreover, some studies show that the phase of emitted harmonics is greatly influenced by the harmonic emission time and the carrier-envelope phase of the driving laser pulse [29, 30]. The fundamental motivation behind the enhancement of the harmonics (in both the cutoff and the intensity) is

the generation of an intense *single attosecond pulse* instead of the attosecond pulse train [31–37].

The harmonics at the cutoff of the HHG spectrum are emitted in a short time with a relatively constant phase. The superposition of these harmonics can lead to the generation of an isolated attosecond pulse [38–41]. On the other hand, the harmonics lie in the plateau region are generated by two primary electron paths (the so-called short and long paths) having two clearly distinguished ionization and recombination times. The superposition of these plateau harmonics leads to a short light burst of sub-femtosecond or attosecond duration separated by twice the laser frequency and for a multi-cycle driving pulse, the superposition of plateau harmonics is observed to produce an attosecond pulse train [42, 43].

The typical shape of the sinc function makes it very interesting from the perspective of the generation of higher-order harmonics. The sinc pulse has a flattop spectral distribution, and also has a single relatively extreme field amplitude which can assist in accelerating the electron to achieve higher kinetic energies. If the electron recombines with the parent ion, then the excess energy will be emitted in the form of energetic pho-

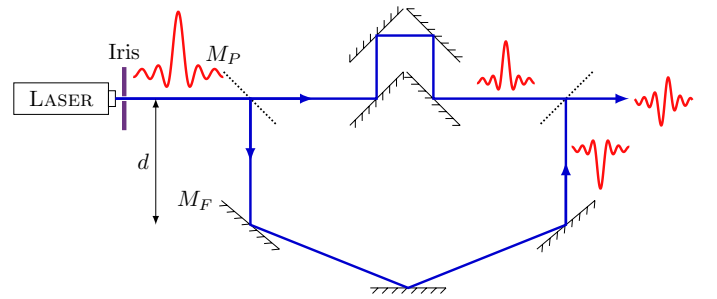


FIG. 1. Schematic diagram representing the proposed experimental setup. In this setup  $M_P$  and  $M_F$  are respectively mirrors with 50% (beam splitter) and 100% reflectivity. The configuration of an odd number of mirrors in the bottom arm is used to rotate the polarization of the pulse by  $180^\circ$ . In the top arm, even number of mirrors are used to induce the desired path difference such that the pulse delay  $\tau = 0$  would correspond to the out of phase addition of both pulses after the second beam splitter.

<sup>\*</sup> ramrajpoot3@gmail.com

<sup>†</sup> amol.holkundkar@pilani.bits-pilani.ac.in

<sup>‡</sup> jnbandyo@gmail.com

tons. The pulse shaping techniques such as *optical frequency combs* are around the corner for approximately three decades [44, 45]. However, after the advent of the *optical arbitrary waveform generation*, the pulse shaping is mainly achieved by the train of identical optical pulses produced by the mode-locked lasers [46]. These mode-locked lasers might have the pulse duration of a few femtoseconds with a repetition rate of a few gigahertz. In order to produce an arbitrary optical waveform, one needs a pulse shaper which can be updated for each pulse. This facet of pulse shaping is actively worked upon by various researchers in the laser fraternity. We believe that the sinc pulses can be generated by the state of the art pulse shaping techniques such as deformable mirrors, a spatial light modulator, an acousto-optic modulator, and many more. By directly synthesizing rectangular shaped and phase-locked frequency comb, researchers have reported the generation of the sinc shaped pulses of exceptional quality [47]. The contemporary technological advances further increase the feasibility aspects of high power sinc shaped pulses in the near future.

In this work, we discuss a simple setup using the sinc laser pulse(s), which promises a *highly tunable* harmonic cutoff in similar intensity ranges. This, in turn, translates to the realization of the tunable radiation source having the photon energies ranging from XUV to soft-Xrays of the electromagnetic spectrum. The theoretical and simulation aspects of the work are discussed in Sec. II, followed by the results and discussion in Sec. III and concluding remarks are made in Sec. IV.

## II. THEORY AND SIMULATION DETAILS

The schematic diagram representing the setup is presented in Fig. 1. A single sinc pulse is passed through the beam splitter and that divided into two parts along different directions. One of the pulses acquires a phase of  $180^\circ$  due to an odd number of reflections from mirrors, and then interferes with the other pulse [48]. The distance  $d$ , as shown in the figure (mirrors assembly in the bottom arm), can easily be tweaked on an optical bench, which in turn induces a path difference between the two pulses and that results in a delay between the pulses. This indicates that the delay parameter can be tuned easily. We will see that the delay between two pulses indeed causes a shift in the harmonic cutoffs. The temporal profile of the electric field of the synthesized pulse is then represented as:

$$E(t) = E_0(\tau) \left[ \frac{\sin[\omega_0(t - t_0 - \tau)]}{\omega_0(t - t_0 - \tau)} - \frac{\sin[\omega_0(t - t_0)]}{\omega_0(t - t_0)} \right], \quad (1)$$

where the laser frequency  $\omega_0 = 0.057$  a.u.,  $\tau$  is the delay between the pulses,  $E_0(\tau)$  is a delay dependent field amplitude, and  $t_0$  introduces some constant phase. Note that,  $\tau = 0$  corresponds to the out of phase addition of the pulses which results in  $E(t) = 0$  [refer Fig. 1]. Irrespective of the delay parameter  $\tau$ , the pulse energy ( $\sim \int |E(t)|^2 dt$ ) can be fixed at some constant value by tweaking the amplitude  $E_0(\tau)$  using the Iris [49]. It should also be noted that  $\tau$  can easily be tuned by varying the distance  $d$  on an optical bench. Throughout the

manuscript, we will be using the atomic units unless otherwise stated; this implies  $e = \hbar = m_e = 1$ .

We study the interaction of the synthesized laser pulse with the *He* atom by numerically solving the one-dimensional time-dependent Schrödinger equation (TDSE) based on the single-active electron (SAE) approximation [50]. The TDSE in the length gauge is written as [51]:

$$\left[ -\frac{1}{2} \frac{\partial^2}{\partial x^2} + V(x) + xE(t) \right] \Psi(x, t) = i \frac{\partial}{\partial t} \Psi(x, t), \quad (2)$$

where  $E(t)$  is the laser field as given by Eq. 1 and  $V(x) = -1/\sqrt{x^2 + \xi}$  is the ionic soft-core potential where the constant  $\xi$  is dependent on the ionization potential of the atom under study. For Helium atom  $\xi = 0.484$  is considered. The TDSE is solved numerically by adopting the split-operator method [52] in which the evolution operator factored as a product of the kinetic and potential energy propagators. The initial ground state is estimated by the imaginary-time propagation method [53] and then starting from this initial state, the time-dependent wavefunction is obtained by solving the TDSE. The time-dependent dipole acceleration  $\ddot{d}(t)$  is calculated using the Ehrenfest theorem as [54]:

$$\ddot{d}(t) = -\langle \Psi(x, t) | \frac{\partial V(x)}{\partial x} + E(t) | \Psi(x, t) \rangle. \quad (3)$$

The harmonic spectrum is then finally be obtained by the Fourier transformation of  $\ddot{d}(t)$ , i.e.,

$$S(\omega) = \left| \frac{1}{\sqrt{2\pi}} \int \ddot{d}(t) \exp[-i\omega t] dt \right|^2. \quad (4)$$

In our calculation, the simulation domain is confined in a finite space of 4000 a.u. where the grid spacing  $\delta x = 0.05$  a.u. The simulation time step is decided from the relation  $\delta t \sim (\delta x)^2/2$ . In order to avoid the reflection of the electron wave packet from the boundaries, an absorbing boundary of thickness 200 a.u. was placed at  $x = \pm 1800$  a.u. The absorption is implemented using the exterior complex scaling method [55]. The convergence of the calculation is checked by varying the grid parameters.

The attosecond pulse is obtained by superposing several harmonics as [56]:

$$I(t) = \left| \sum_q a_q \exp[iq\omega t] \right|^2, \quad (5)$$

where  $q$  is the harmonic order and  $a_q$  represents the inverse Fourier transformation given as:

$$a_q = \frac{1}{\sqrt{2\pi}} \int \ddot{d}(t) \exp[-iq\omega t] dt. \quad (6)$$

The time-frequency analysis has been done to get insight of the quantum recollision processes. The wavelet transform has been performed using the standard Gabor time-frequency analysis [57, 58].

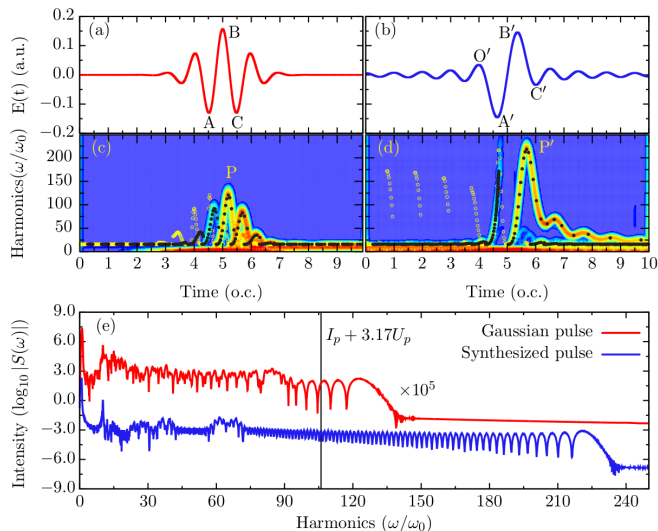


FIG. 2. The electric fields of the 800 nm/5 fs Gaussian-envelope pulse (a) and synthesized pulse with parameter  $\tau = 0.71T$  (b) are presented. We presented the corresponding classical ionizing and returning energy maps along with the time-frequency distributions of the HHG spectra in (c) and (d) respectively for Gaussian and synthesized pulse. However, the harmonic spectra for both cases are compared in (e). For the purpose of clarity, the harmonic intensity of the Gaussian pulse is multiplied by a factor of  $10^5$ . The cutoff as predicted by the 3 step model is also shown as a vertical line ( $106\omega_0$ ) in (e).

### III. RESULTS AND DISCUSSIONS

In the following, we compare the harmonic spectrum by a Gaussian laser pulse and the synthesized pulse given by Eq. 1, followed by the effect of the delay  $\tau$  on the harmonic cutoffs, and finally its impact on the generation of the optimal attosecond pulses.

#### A. Comparison with Gaussian Pulse

Initially, in order to show the preeminence of our synthesized pulse for the generation of higher-order harmonics, we have compared the HHG spectra generated by the synthesized laser field defined in Eq.1 and the 800 nm/5 fs Gaussian-enveloped laser pulse. The temporal profile of the Gaussian laser pulse is given as:

$$E_g(t) = E_{0g} \exp\left[-4\ln 2 \frac{t^2}{\tau_g^2}\right] \cos(\omega_0 t), \quad (7)$$

where  $E_{0g}$  is the amplitude of the laser field, and  $\omega_0 (= 0.057$  a.u.) is the laser frequency same as used in the synthesized pulse, and  $\tau_g = 5$  fs is considered. It should be noted that the pulse energy of both the pulses is fixed at the value  $\sim 1.91$  a.u. Thus the peak field amplitude for the Gaussian pulse is estimated to be  $E_{0g} \sim 0.1567$  a.u. However, the field amplitude of the synthesized pulse is considered to be  $E_0 \sim 0.1453$  a.u.

The temporal electric field profile of the Gaussian-envelope and the synthesized pulse is presented in Fig. 2(a) and 2(b), respectively. For the synthesized pulse, the delay parameter  $\tau$  is chosen to be  $0.71T$ , where  $T (= 2\pi/\omega_0)$  is the time corresponding to one optical cycle (o.c.). Compared to the case of the Gaussian pulse, we can see that the laser cycle of the synthesized pulse is expanded. The electron ionized around the negative maximum of the synthesized laser field can gain higher energies in the relatively longer acceleration process, and consequently the harmonics with larger cutoff energy would then be achieved when it will recombine with the parent ion. The comparison among the HHG power spectra of atomic He for the Gaussian and the synthesized pulse is presented in Fig. 2(e). The differences in harmonic intensities among the two curves in the plateau region are actually small, so for the purpose of clarity we have shifted the harmonic signal for the Gaussian pulse along the y-axis. These harmonic spectrum have the characteristic structure of a typical HHG spectra, i.e., irregular behavior towards the lower harmonics region, then gradually it becomes regular within the plateau region, and finally a sudden drop in the harmonic intensity at the *cutoff*. The results show that the harmonic cutoff is impressively extended from  $140\omega_0$  for the Gaussian field to  $235\omega_0$  for the synthesized field. The harmonic structure in the supercontinuum region of the synthesized field is less modulated than the case of Gaussian field. This condition is favorable for the generation of isolated attosecond pulse. The cutoff rule [59]  $I_p + 3.17U_p$  (where  $U_p = E^2/4\omega_0^2$  is the quiver energy, and  $I_p = 0.904$  a.u. is the ionization potential for the He atom) for the maximum possible harmonic photon energy predicts the cutoff at  $106\omega_0$  (164 eV), while the harmonic cutoff for the case of synthesized pulse is observed at  $235\omega_0$  (364 eV). This inability of three steps model to predict the harmonic cutoff is due to the classical consideration of the fact that the laser pulse intensity should be constant during the quiver motion of electron [17, 40]. Since the laser intensity in

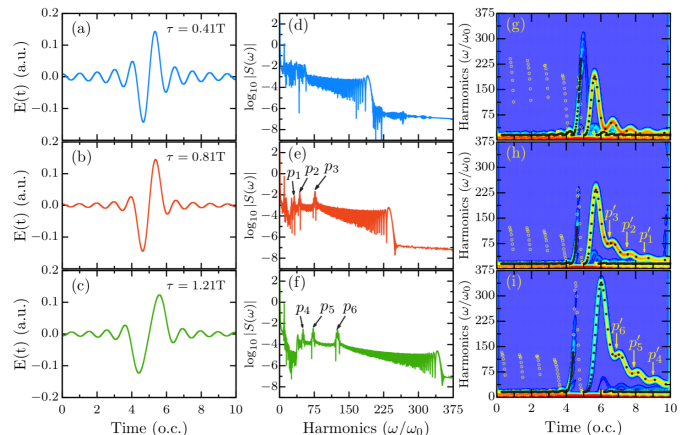


FIG. 3. Temporal profile of the electric field with delay parameter  $\tau = 0.41T$  (a),  $0.81T$  (b), and  $1.21T$  (c). Corresponding harmonic spectra are respectively presented in (d), (e) and (f). Time frequency analysis of the electron quantum path along with the classical ionization and recombination time are shown in (g), (h) and (i) respectively.

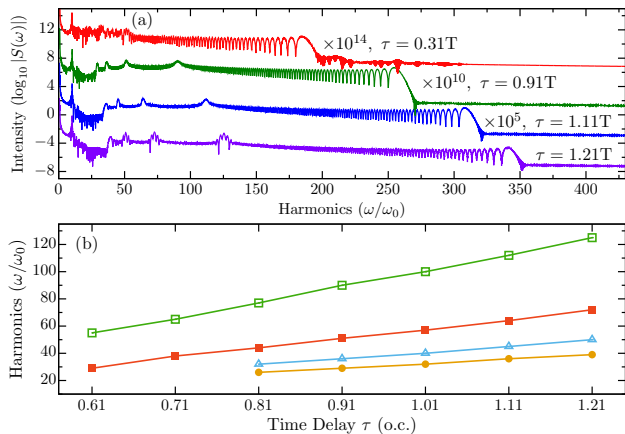


FIG. 4. The HHG spectra of synthesized pulse for different delay cases are presented (a). For the purpose of clarity, the harmonic intensities of  $\tau = 0.31T$ ,  $0.91T$  and  $1.11T$  pulses are multiplied by factors of  $10^{14}$ ,  $10^{10}$  and  $10^5$ , respectively. We have also presented the specific enhanced harmonics driven by synthesized pulse for different delay cases in (b).

our case changes significantly in one laser cycle, we can not expect that the celebrated three steps model would predict the harmonic cutoff correctly.

Both the classical theory [9] and quantum time-frequency analysis are adopted to have a deeper understanding of the generation of the higher-order harmonics. In Figs. 2(c) and 2(d), we show the classical electron trajectories along with the time-frequency distribution of the HHG spectra for the above two cases. In the case of the synthesized field, the electron trajectory map shows two paths with different emission times (solid black circles) contributing to each harmonic in HHG spectra [refer Fig.2(d)]. The two branches of the emission time trajectory with positive and negative slopes are corresponding to the short and long paths, respectively. Likewise, in the time-frequency profile, there are two quantum paths contributing to each of the harmonic within half of the optical cycle of the synthesized laser field. It should be noted that the maximum harmonic order corresponding to the Gaussian pulse, marked by the point  $P$  in Fig. 2(c), is approximately equal to  $140\omega_0$ ; whereas, the maximum harmonic order corresponding to the synthesized pulse, marked as  $P'$  in Fig. 2(d), is observed at the value  $235\omega_0$ . Even though the field energy content of both the driving pulses are the same, but the order of the cutoff harmonic corresponding to the synthesized pulse is about  $95\omega_0$  (or  $147$  eV) more than the same corresponding to the Gaussian pulse. The harmonic spectrum for these cases is illustrated in Fig. 2(e), which complement the results presented using the time-frequency analysis.

Based on the classical trajectory maps, we can state that the peak  $P$  is originated by the  $ABC$  process marked in Fig. 2(a). The electron gets ionized by tunneling when the magnitude of the laser field amplitude reaches its maxima around the point  $A$ , then it gets accelerated by the next maxima at  $B$  which results in gaining high kinetic energy, and finally the electron recombines with the parent ion core in between the peak at  $B$

and the dip at  $C$ , which results in the emission of harmonic photons up to the order of 135. The maximum energy at the peak  $P$  is determined by the kinetic energy gained by the electron during the acceleration process. On the contrary, in the case of the synthesized field [refer Fig. 2(b)], the laser cycle is expanded, and therefore the electrons get ionized around  $A'$ . The free electron then accelerates for a relatively long time till the peak  $B'$ . Then it returns to the core ion with higher kinetic energy in between  $B'$  and  $C'$  and recombines with the ion. The recombination process leads to the emission of harmonics up to the order of 235.

## B. Effect of Delay on HHG and Scaling law

We now show how the synthesized pulse waveform resulting from the time delay ( $\tau$ ) between two-component sinc pulses affects the resulting HHG spectra. The temporal profiles of the synthesized pulse for different time delays  $\tau = 0.41T$ ,  $0.81T$ , and  $1.21T$  are respectively presented in Figs. 3(a) - 3(c). The effect of the increasing delay on field strength can be seen as an extension in the laser cycle. The respective harmonic spectra [refer Eq. 4] for these delay parameters are presented in Figs. 3(d)-3(f). The harmonic cutoff energies for these delays are observed respectively at  $202\omega_0$ ,  $245\omega_0$ , and  $350\omega_0$ . Furthermore, one important feature is observed in the harmonic spectrum presented in Figs. 3(e) and 3(f) is the enhancement in HHG yield of harmonics around the peaks  $p_1$ ,  $p_2$ ,  $p_3$  marked in Fig. 3(e) and the peaks marked as  $p_4$ ,  $p_5$ ,  $p_6$  in Fig. 3(f). The underlying mechanism behind the extension of the HHG cutoff energy and the selective harmonic yield can be understood from the classical trajectories and the quantum time-frequency analysis of the quantum paths of the electron, as shown in Figs. 3(g)-3(i). Here, the classical trajectory analysis shows how the effect of the time dependence of electron kinetic energy on the ionization (yellow circles) and also on the recombination (solid black circles) times.

The classical electron trajectories are consistent with the results of the time-frequency analysis of the electron quantum paths. The increasing delay time ( $\tau$ ) results in the broadening of both negative and positive cycle of the synthesized

TABLE I. Summary of harmonic cutoffs ( $\omega_c$ ) for different delay parameters ( $\tau$ ) are presented along with their respective intensities ( $\log_{10} |S(\omega_c)|$ ). The enhanced harmonics ( $\omega_{en}$ ) are also summarized in last column and their respective intensities in multiple ( $\eta$ ) of their cutoff intensity are mentioned in the bracket. All the harmonics are presented in units of the fundamental frequency  $\omega_0$ .

$\tau$ [T]	$\omega_c$	$\log_{10}  S(\omega_c) $	$\omega_{en}(\eta)$
0.81	248	-3.18	26(8), 32(14), 44(24), 77(35)
0.91	271	-3.33	29(4), 36(7), 51(11), 90(10)
1.01	291	-3.58	32 (2), 40(3), 57(5), 100(5)
1.11	320	-4.00	36(5), 45(14), 64(21), 112(17)
1.21	350	-4.55	39(33), 50(112), 72(132), 125(85)

laser field. This eventually modifies the ionization and recombination time, and also the kinetic energy of returning electron. The increased electron kinetic energy will cause an enhancement in the emitted harmonic photon energy as shown in Figs. 3(g)-3(i). Furthermore, relatively higher intensities of harmonics around the peaks at  $p_1$ ,  $p_2$  and  $p_3$  in Fig. 3(e) can be understood by the respective time-frequency analysis as shown in Fig. 3(h), where the corresponding plateaus are marked as  $p'_1$ ,  $p'_2$  and  $p'_3$ . As can be seen that the harmonic emissions for the same harmonics ( $p_1$ ,  $p_2$  and  $p_3$ ) are taking place for relatively longer time. Similarly, in Fig. 3(i), the harmonics at plateaus  $p'_4$ ,  $p'_5$  and  $p'_6$  are getting emitted for relatively longer time, giving higher yield of those selected harmonics as shown around the peaks at  $p_4$ ,  $p_5$  and  $p_6$  in Fig.3(f).

The harmonic spectrum for different delay parameters is presented in Fig. 4(a). Not only the harmonic cutoff changes with the delay parameter  $\tau$ , but some harmonic components are also observed to be enhanced as compared to the neighboring harmonics in the plateau region. In Fig. 4(b), we have presented the location of enhanced harmonics as a function of the delay parameter. The position of the enhanced harmonics in the plateau region of the spectrum is found to be changing for different time delays. The intensity of these harmonics are about one order of magnitude higher than the surrounding harmonics. The mechanism behind these selective enhancement has already been discussed above. These enhanced harmonics can be used further as a monochromatic source for many important applications, which include the seeding of an XUV free-electron laser or laser-plasma amplifiers [60]. In Table I, we have presented some typical harmonic cutoffs and their intensities for different values of the delay  $\tau$ . Here we have also presented some enhanced harmonics and their intensities as a multiple of the intensity observed at the harmonic cutoffs.

Figure 5(a) depicts the variation in the peak field amplitude  $E_0(\tau)$  of the *component sinc pulse* which is defined in Eq. 1. Here the energy of the *synthesized pulse* are also presented for different time delays. The curves have been normalized with respect to the values for the case of  $\tau = 0.71T$ . One can see that the pulse energy is fixed for all the delay cases, while the peak field amplitude increases on either side of the delay  $\tau = 0.71T$  case. It should be noted that for  $\tau < 0.71T$ , the overlap of the central peaks of the oppositely polarized fields demands higher pulse intensity to keep the pulse energy constant. This results in relatively rapid increase in the peak amplitude in  $\tau < 0.71T$  cases. In Fig. 5(b), the observed harmonic cutoff  $\omega_c/\omega_0$  for different delay parameters ( $\tau$ ) is presented and based on these observations, we infer that the HHG cutoff in the current setup scales as  $\sim \tau^{5/2}$  for a fixed driver pulse energy. The scaling law is consistent upto some large time delay such as 1.31T. Moreover, the increase in delay deforms the synthesized pulse by inducing local field maximum between the two central peaks of the field. The intensities of the respective harmonic cutoff for different delay parameters are also illustrated in Fig. 5(b). It is observed that the cutoff intensities ( $\log_{10}|S(\omega_c)|$ ) follow a  $\sim -\tau^5$  scaling. The decrease in HHG yield can be explained by taking into account the spreading of electronic wave-packet during propagation

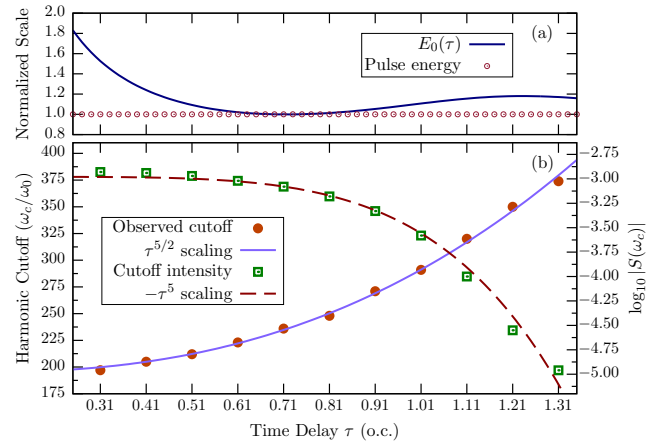


FIG. 5. The variation in the peak field amplitude  $E_0(\tau)$  with delay parameter is presented along with the pulse energy. Field amplitude and pulse energy ( $\propto \int |E(t)|^2 dt$ ) are normalized with respect to values associated with the delay parameter  $\tau = 0.71T$ . The peak field amplitude and the pulse energy for  $\tau = 0.71T$  are considered to be respectively  $\sim 0.1453$  a.u. and  $\sim 1.91$  a.u. The respective observed harmonic cutoff (solid circles) with the  $\sim \tau^{5/2}$  scaling (solid curve) for different time delays is presented (b). The variation in harmonic cutoff intensity (squares) with the delay parameter  $\tau$  is also shown along with the  $\sim -\tau^5$  (dashed line) scaling (b).

in the continuum. As mentioned earlier, increasing the delay in pulse synthesis will result in elongation in the laser cycle. Since the wave-packet propagation time in the continuum is proportional to the laser cycle, the wave-packet has more time to spread with increasing delay, thus scaling down the efficiency of the recombination process in harmonic emission.

These scaling laws for harmonic cutoff and their respective intensities clearly demonstrate the utility of this setup. We not only predict the harmonic cutoff, but also its intensity in terms of the time delay between two oppositely polarized sinc

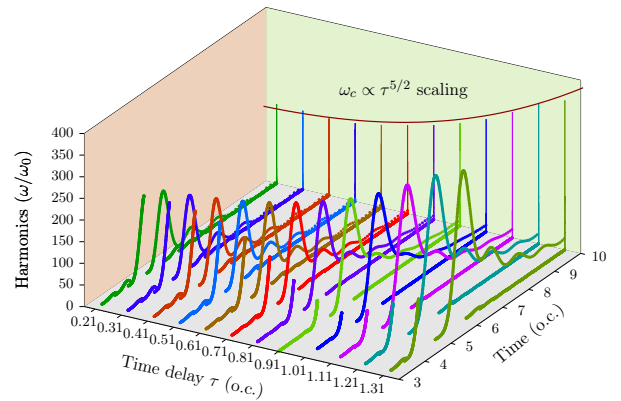


FIG. 6. Classical trajectories are presented for different delay parameters and again the  $\omega_c \propto \tau^{5/2}$  scaling is also projected. All other laser parameters are same as presented in Fig. 5.

pulses. The above mentioned scaling law of the harmonic cutoff energy is also validated using the classical trajectory analysis and the corresponding returning electron trajectory maps are presented in Fig. 6. Even though there is no way to comment on the cutoff intensities from the classical analysis, but the scaling property of the maximum radiated photon energy can be predicted promisingly. It is clear from Fig. 6 that, for smaller time delays (i.e.,  $\tau < 0.41T$ ), the cutoff harmonics are emitted due to the ionization around the peak marked as  $O'$  in Fig. 2(b)] of the synthesized laser pulse. The electrons ionize around the peak at  $O'$  and later recombine between the dip at  $A'$  and the peak at  $B'$ . These electrons accelerate for relatively longer times as compared to the electrons ionized around the dip at  $A'$  and recombined between the peak at  $B'$  and the dip at  $C'$ . Therefore, the energy of the emitted photons are higher for the former case.

Moreover, with the increasing delay, the width of the dip at  $A'$  and the peak at  $B'$  increases, and concurrently the amplitude of the peak at  $O'$  decreases [refer Fig. 3(a)-3(c)]. As a result, the cases for which  $\tau$  is greater than  $0.41T$ , the quiver energy of the electrons ionized around the peak at  $O'$  decreases, while for the electrons ionize around the dip at  $A'$  would return with higher kinetic energies as observed in Fig. 6. The typical nature of the sinc pulse yields the previously mentioned scaling of the cutoff energy and its intensity in the harmonic spectrum. The delay parameter actually controls the interference between the two pulses of opposite polarization, which eventually translates into the modification of the electron quantum path as well as the recombination energy of the returning electron.

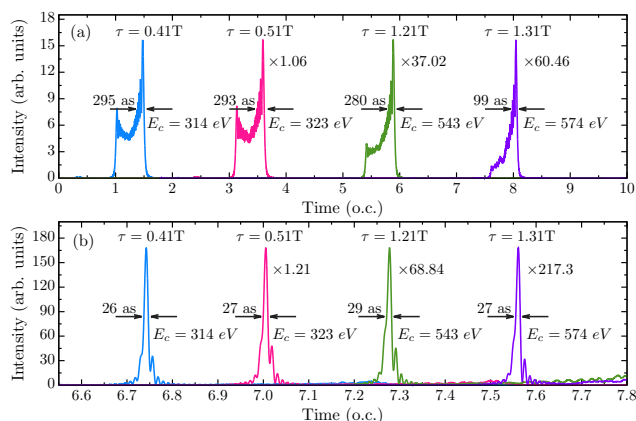


FIG. 7. The temporal profiles of the attosecond pulses generated by properly selecting the filtering window of 100 harmonics before cutoff for time delays  $\tau = 0.41T, 0.51T, 1.21T$ , and  $1.31T$ : without (a) and with (b) phase compensation is presented. For the purpose of clarity, the ASPs are shifted in time scale and multiplied by some factors as shown.

### C. Optimal attosecond pulse generation

We now discuss the role of the higher order harmonics in the generation of a single attosecond pulse. In Fig. 5, we observe nice scaling behavior of the harmonic cutoff and their respective intensity in terms of the delay parameter  $\tau$ . We now study how to generate an attosecond pulse (ASP) by filtering several harmonics just before the cutoff but in the plateau region. The temporal profile of the ASP for a given delay parameter are obtained by superposing the contribution of the different harmonics and then performing the inverse Fourier transform [refer Eq. 5]. In Fig. 7(a), we present isolated attosecond pulses generated without any phase compensation, but just by superposing the last 100 harmonics up to the cutoff of the harmonic spectrum corresponding to a bandwidth of  $\sim 155$  eV for different delay parameters. The pulses have been emitted within the same optical cycle, but just for the sake of clear presentation, we have shifted the pulses along time scale. The maximum harmonic photon energy for different ASPs corresponding to delay  $\tau = 0.41T, 0.51T, 1.21T$  and  $1.31T$  are 314 eV, 323 eV, 543 eV and 574 eV, respectively [refer Fig. 5]. The generated ASPs become shorter with increasing values of the delay parameter. Here we show that, as we increase the delay from  $\tau = 0.41T$  to  $\tau = 1.31T$ , the pulse width of the generated ASPs decrease from 295 as to 99 as. We explain this behavior using Figs. 3(g)-3(i). Here we see that as we increase the delay, the intensity of the short trajectory diminishes. This indicates that the contribution of the harmonics due to the shorter trajectories is very less in the HHG spectrum. Therefore, in the formation of attosecond pulses, the harmonics corresponding to the longer trajectories are present, and that results in the shorter ASP. It should be noted that, by the nature of the synthesized pulse, harmonic emission takes place only for a single cycle of the driving pulse. Therefore, we have a single ASP instead of a pulse train upon the superposition of a large range of harmonics of the HHG spectrum. The single ASP is more promising for applications in time-resolved spectroscopy. This method reduces the need to adopt various gating techniques [61] to obtain the single ASP rather than pulse train.

The harmonics in the HHG process are emitted over a range of time, which means the phase of each harmonic is arbitrary. As a result, the superposition of entire plateau harmonics can not generate the shortest attosecond pulse. However, the phase dispersion can be compensated by propagating the ASP through either a gas medium or a thin metal foil [37, 62]. In our simulations, the harmonic phase has been compensated by taking a constant phase difference between two consecutive harmonics, and the corresponding results are shown in Fig. 7(b). After the phase compensation, intense isolated attosecond pulses with durations (photon energy) of 26 as (314 eV), 27 as (323 eV), 29 as (543 eV) and 27 as (574 eV) can be achieved for time delays  $\tau = 0.41T, 0.51T, 1.21T$  and  $1.31T$ , respectively. Moreover, the intensity of attosecond pulses has been increased up to one order of magnitude compared to the scenario without any phase compensation.

One can notice that despite having a large harmonic continuum in the case of the synthesized field, the generated at-

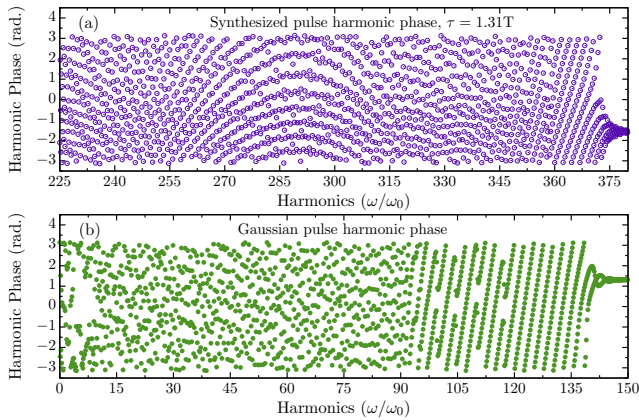


FIG. 8. Phase of emitted harmonics in case of : (a) Synthesized pulse with delay  $\tau = 1.31T$  and (b) Gaussian-envelope pulse with laser parameters same as taken in Fig. 2(a).

to second pulse is not as short as it is in the case of a Gaussian pulse [20]. This can be understood by taking into account the variation of the phases of the emitted harmonics. A comparison between the emitted harmonic phases for synthesized and Gaussian pulse is depicted in Fig. 8(a) and 8(b), respectively. We see that, for the synthesized pulse, the previous 15 harmonics from the cutoff (between 360th - 375th order) have constant phase variation between consecutive harmonics; while for the Gaussian pulse, nearly 50 harmonics (between 90th - 140th order) are separated by a constant phase. The superposition of these phase-locked harmonics can generate an ASP of shorter duration without applying any phase compensation technique. However, if the phase dispersion is properly compensated, then the obtained large HHG continuum in case of the synthesized pulse can be used to produce a shorter ASP.

#### IV. CONCLUDING REMARKS

We have theoretically investigated the higher harmonic generation and the generation of a single attosecond pulse from a He atom. The driving field is sculpted from a sinc-shaped pulse by a simple experimentally realizable setup. This syn-

thesized field can be considered as a single cycle pulse which can favorably control the electron quantum path. It has been observed that, in comparison with a few-cycle Gaussian pulse of the same energy, the bandwidth of an XUV supercontinuum spectrum is significantly broadened for the synthesized pulse. We find that the energy of the cutoff harmonics increases with the increasing delay parameter ( $\tau$ ). Specifically, it nicely scales as  $\sim \tau^{5/2}$  for a fixed driver pulse energy. Furthermore, the intensity of the cutoff harmonic is also seen to be following a  $\sim -\tau^5$  scaling. These well-defined scaling laws for the harmonic cutoff and its intensity indicate a realizable experimental setup, wherein radiations from XUV to soft-X-rays can be generated by simply changing the distance  $d$  on an optical bench [refer Fig. 1].

We have used these higher harmonics to generate attosecond pulses having a central frequency in XUV to the soft-X-ray regime of the electromagnetic spectrum. This has been achieved by filtering the harmonics of bandwidth 155 eV from the respective harmonic cutoff for a given delay parameter. The quantum time-frequency analysis shows that the contribution of the harmonics corresponding to the shorter quantum path in the HHG supercontinuum spectrum decreases with the increasing delay in the pulse synthesis. As a result, an isolated  $\sim 100$  as pulse for  $\tau = 1.31T$  is straightforwardly obtained without any phase compensation. If the phase is compensated correctly, then an intense ultrashort  $\sim 27$  as pulse can be generated with photon energy  $\sim 570$  eV. The advantage of the scheme proposed here lies in the tuning of broadband XUV supercontinuum by merely adjusting the time delay, which seems feasible from an experimental point of view. The enhancement in some satellite harmonics is also studied, and its dependence on delay parameter  $\tau$  has been summarized. Exploration of higher dimensional effects on the electron quantum path and the corresponding attosecond pulse generation using this synthesized sinc pulse is reserved for the future project.

#### ACKNOWLEDGMENTS

Authors acknowledge the Science and Engineering Research Board, Department of Science and Technology, Government of India, for funding the project EMR/2016/002675.

- 
- [1] M. F. Ciappina, J. A. Pérez-Hernández, A. S. Landsman, W. A. Okell, S. Zherebtsov, B. Förg, J. Schötz, L. Seiffert, T. Fennel, T. Shaaran, T. Zimmermann, A. Chacón, R. Guichard, A. Zaïr, J. W. G. Tisch, J. P. Marangos, T. Witting, A. Braun, S. A. Maier, L. Roso, M. Krüger, P. Hommelhoff, M. F. Kling, F. Krausz, and M. Lewenstein, *Rep. Prog. Phys.* **80**, 054401 (2017).
  - [2] K.-J. Yuan and A. D. Bandrauk, *Phys. Rev. Lett.* **110**, 023003 (2013).
  - [3] L. Medišauskas, J. Wragg, H. van der Hart, and M. Y. Ivanov, *Phys. Rev. Lett.* **115**, 153001 (2015).
  - [4] M. Chini, K. Zhao, and Z. Chang, *Nat. Photon.* **8**, 178 (2014).
  - [5] F. Krausz and M. Ivanov, *Rev. Mod. Phys.* **81**, 163 (2009).
  - [6] P. B. Corkum and F. Krausz, *Nat. Phys.* **3**, 381 (2007).
  - [7] P. M. Paul, E. S. Toma, P. Breger, G. Mullot, F. Augé, P. Balcou, H. G. Muller, and P. Agostini, *Science* **292**, 1689 (2001).
  - [8] F. Calegari, G. Sansone, S. Stagira, C. Vozzi, and M. Nisoli, *J. Phys. B: At. Mol. Opt. Phys.* **49**, 062001 (2016).
  - [9] P. B. Corkum, *Phys. Rev. Lett.* **71**, 1994 (1993).
  - [10] M. Lewenstein, P. Balcou, M. Y. Ivanov, A. L'Huillier, and P. B. Corkum, *Phys. Rev. A* **49**, 2117 (1994).
  - [11] H. Liu, L.-Q. Feng, and H. Liu, *Opt. Commun.* **441**, 55 (2019).
  - [12] D. Peng, M. Frolov, L.-W. Pi, A. F. Starace, *et al.*, *Phys. Rev. A* **97**, 053414 (2018).

- [13] L. Feng and H. Liu, *Mol. Phys.* **115**, 1562 (2017).
- [14] H. Liu, R. L. Q. Feng, and R. S. Castle, *Laser Phys.* **29**, 035302 (2019).
- [15] J.-X. Han, J. Wang, Y. Qiao, A.-H. Liu, F.-M. Guo, and Y.-J. Yang, *Opt. Express* **27**, 8768 (2019).
- [16] M. Lara-Astiaso, R. E. F. Silva, A. Gubaydullin, P. Rivière, C. Meier, and F. Martín, *Phys. Rev. Lett.* **117**, 093003 (2016).
- [17] J. Zhou, J. Peatross, M. M. Murnane, H. C. Kapteyn, and I. P. Christov, *Phys. Rev. Lett.* **76**, 752 (1996).
- [18] R. A. Ganeev, C. Hutchison, T. Witting, F. Frank, S. Weber, W. A. Okell, E. Fiordilino, D. Cricchio, F. Persico, A. Zair, J. W. G. Tisch, and J. P. Marangos, *J. Opt. Soc. Am. B* **30**, 7 (2013).
- [19] Z. Chang, *OSA Continuum* **2**, 2131 (2019).
- [20] R.-F. Lu, H.-X. He, Y.-H. Guo, and K.-L. Han, *J. Phys. B: At. Mol. Opt. Phys.* **42**, 225601 (2009).
- [21] L.-q. Feng and H. Liu, *Chin. J. Chem. Phys.* **28**, 21 (2015).
- [22] C. Jin and C. D. Lin, *Chin. Phys. B* **25**, 094213 (2016).
- [23] Y. Wang, H. Wu, Y. Chen, Z. Lu, C. Yu, Q. Shi, K. Deng, and R. Lu, *AIP Adv.* **2**, 022102 (2012).
- [24] G. Orlando, P. P. Corso, E. Fiordilino, and F. Persico, *J. Phys. B: At. Mol. Opt. Phys.* **43**, 025602 (2009).
- [25] F. Wang, W. Liu, L. He, L. Li, B. Wang, X. Zhu, P. Lan, and P. Lu, *Phys. Rev. A* **96**, 033407 (2017).
- [26] I. Yavuz, M. F. Ciappina, A. Chacón, Z. Altun, M. F. Kling, and M. Lewenstein, *Phys. Rev. A* **93**, 033404 (2016).
- [27] L. Feng, *Phys. Rev. A* **92**, 053832 (2015).
- [28] H. Yuan, F. Li, and H. Long, *J. Opt. Soc. Am. B* **34**, 2390 (2017).
- [29] A. de Bohan, P. Antoine, D. B. Milošević, and B. Piraux, *Phys. Rev. Lett.* **81**, 1837 (1998).
- [30] K. J. Schafer, M. B. Gaarde, A. Heinrich, J. Biegert, and U. Keller, *Phys. Rev. Lett.* **92**, 023003 (2004).
- [31] K.-J. Yuan and A. D. Bandrauk, *Phys. Rev. Lett.* **110**, 023003 (2013).
- [32] M. A. Khokhlova and V. V. Strelkov, *Phys. Rev. A* **93**, 043416 (2016).
- [33] M. Dashcasan, *Opt. Commun.* **318**, 216 (2014).
- [34] Z. Zeng, Y. Leng, R. Li, and Z. Xu, *J. Phys. B At. Mol. Opt. Phys.* **41**, 215601 (2008).
- [35] E. Goulielmakis, M. Schultze, M. Hofstetter, V. S. Yakovlev, J. Gagnon, M. Uiberacker, A. L. Aquila, E. M. Gullikson, D. T. Attwood, R. Kienberger, F. Krausz, and U. Kleineberg, *Science* **320**, 1614 (2008).
- [36] K. Zhao, Q. Zhang, M. Chini, Y. Wu, X. Wang, and Z. Chang, *Opt. Lett.* **37**, 3891 (2012).
- [37] R. López-Martens, K. Varjú, P. Johnsson, J. Mauritsson, Y. Mairesse, P. Salières, M. B. Gaarde, K. J. Schafer, A. Persson, S. Svanberg, C.-G. Wahlström, and A. L'Huillier, *Phys. Rev. Lett.* **94**, 033001 (2005).
- [38] M. Hentschel, R. Kienberger, C. Spielmann, G. A. Reider, N. Milosevic, T. Brabec, P. Corkum, U. Heinzmann, M. Drescher, and F. Krausz, *Nature* **414**, 509 (2001).
- [39] R. Kienberger, M. Hentschel, M. Uiberacker, C. Spielmann, M. Kitzler, A. Scrinzi, M. Wieland, T. Westerwalbesloh, U. Kleineberg, U. Heinzmann, M. Drescher, and F. Krausz, *Science* **297**, 1144 (2002).
- [40] I. P. Christov, M. M. Murnane, and H. C. Kapteyn, *Phys. Rev. Lett.* **78**, 1251 (1997).
- [41] E. Goulielmakis, M. Uiberacker, R. Kienberger, A. Baltuska, V. Yakovlev, A. Scrinzi, T. Westerwalbesloh, U. Kleineberg, U. Heinzmann, M. Drescher, and F. Krausz, *Science* **305**, 1267 (2004).
- [42] P. Agostini and L. F. DiMauro, *Rep. Prog. Phys.* **67**, 813 (2004).
- [43] P. M. Paul, E. Toma, P. Breger, G. Mullot, F. Augé, P. Balcou, H. Muller, and P. Agostini, *Science* **292**, 1689 (2001).
- [44] S. T. Cundiff and J. Ye, *Rev. Mod. Phys.* **75**, 325 (2003).
- [45] G. Krauss, S. Lohss, T. Hanke, A. Sell, S. Eggert, R. Huber, and A. Leitenstorfer, *Nat. Photon.* **4**, 33 (2009).
- [46] S. T. Cundiff and A. M. Weiner, *Nat. Photonics* **4**, 760 (2010).
- [47] M. A. Soto, M. Alem, M. Amin Shoaie, A. Vedadi, C.-S. Brès, L. Thévenaz, and T. Schneider, *Nat. Commun.* **4**, 2898 (2013).
- [48] E. Neyra, F. Videla, M. F. Ciappina, J. A. Pérez-Hernández, L. Roso, and G. A. Torchia, *Phys. Rev. A* **98**, 013403 (2018).
- [49] V. E. Nefedova, M. F. Ciappina, O. Finke, M. Albrecht, M. Kozlová, and J. Nejdil, *Appl. Phys. Lett.* **113**, 191101 (2018).
- [50] M. Awasthi, Y. V. Vanne, A. Saenz, A. Castro, and P. Decleva, *Phys. Rev. A* **77**, 063403 (2008).
- [51] A. Chacón, M. F. Ciappina, and M. Lewenstein, *Phys. Rev. A* **92**, 063834 (2015).
- [52] M. Feit, J. Fleck, and A. Steiger, *J. Comp. Phys.* **47**, 412 (1982).
- [53] P. Bader, S. Blanes, and F. Casas, *J. Chem. Phys.* **139**, 124117 (2013).
- [54] G. van de Sand and J. M. Rost, *Phys. Rev. Lett.* **83**, 524 (1999).
- [55] F. He, C. Ruiz, and A. Becker, *Phys. Rev. A* **75**, 053407 (2007).
- [56] H. Z. Jooya, P.-C. Li, S.-L. Liao, and S.-I. Chu, *Phys. Lett. A* **380**, 316 (2016).
- [57] A. Koushki, M. Mohsen-Nia, R. Sadighi-Bonabi, and E. Irani, *Comput. Theor. Chem.* **1095**, 104 (2016).
- [58] H. Zhong, J. Guo, W. Feng, P.-C. Li, and X.-S. Liu, *Phys. Lett. A* **380**, 188 (2016).
- [59] J. L. Krause, K. J. Schafer, and K. C. Kulander, *Phys. Rev. Lett.* **68**, 3535 (1992).
- [60] G. Lambert, T. Hara, D. Garzella, T. Tanikawa, M. Labat, B. Carre, H. Kitamura, T. Shintake, M. Bougeard, S. Inoue, *et al.*, *Nat. Phys.* **4**, 296 (2008).
- [61] Y. Huo, Z. Zeng, R. Li, and Z. Xu, *Opt. Express* **13**, 9897 (2005).
- [62] Y. Mairesse, A. de Bohan, L. J. Frasinski, H. Merdji, L. C. Dinu, P. Monchicourt, P. Breger, M. Kovačev, R. Taïeb, B. Carré, H. G. Muller, P. Agostini, and P. Salières, *Science* **302**, 1540 (2003).